Showcasing research from Professor Iyer's laboratory, Department of Chemistry, Indian Institute of Technology Guwahati, Guwahati-781039, Assam, India.

An engineered organic electrochemical transistor (OECT) platform with a highly ammonia-sensitive mesoporous membrane

An OECT-based organic transistor device composed of PEDOT:PSS, presents increased selectivity for ammonia detection at a very low concentration of 71.6 ppb and at remarkably low operating voltages of ≤1 volts at room temperature. Such sensitive and selective behavior towards ammonia even in aqueous environment is attributed to the formation of a smart mesoporous bed (a polyhydroxyl layer). The present approach can be extended to detect other biological and chemical analytes efficiently due to its unique compatibility, electronic properties and cost-effectiveness.

ROYAL SOCIETY
OF **CHEMISTRY**

rsc.li/sensors

PAPER

Check for updates

An engineered organic electrochemical transistor (OECT) platform with a highly ammonia-sensitive mesoporous membrane†

Indrani Medhi[a] and Parameswar Krishnan Iyer [iD] *[ab]

The development of an improved sensor design methodology *via* an organic electrochemical transistor (OECT)-based organic transistor device is presented here. A polyhydroxyl layer is introduced strategically in the OECT sensor assembly which is composed primarily of poly(3,4-ethylenedioxythiophene) doped with polystyrene-sulfonate (PEDOT:PSS). By introducing this layer, an increased selectivity for ammonia compared to other tested analytes in an aqueous environment has been found. A very low order of magnitude of ammonia concentration was detected by this device at very low operating voltages at room temperature. This superior performance of the OECT device is attributed to the formation of a smart mesoporous bed with electronic properties, which helped to obtain 71.6 ppb as the limit of detection (LOD) for ammonia. This approach incorporates an OECT device platform wherein the sensitivity of the sensor system is enhanced such that improved device performance is achieved while maintaining the cost-effectiveness.

Introduction

Although innumerable sensors for ammonia detection are available for use in various industries and environmental monitoring, the sensitivity of the device for medical applications is very important. Particularly, the detection of ammonia present in a very low concentration generated during the course of diseases or human metabolism is challenging. Among several techniques, the hybrid nanostructures formed by blending of nanoparticles of metal/metal-oxides with a polymer or its derivatives have been utilized in estimating environmental hazards.[1–3] These air and environmental monitoring systems can detect analytes within the limit of <1 ppb. Certain optical gas sensors are suitable to detect ammonia but they are large and expensive, and the reagent consumption and maintenance requirements pose additional problems, making them less favorable.[4,5] In this aspect, research on the improvement of sensitivity, selectivity, response time and reliability, and miniaturization and reduction of cost and power consumption are factors to be considered. Nanostructured materials are widely used as gas sensors due to their high volume ratio, good morphology and

excellent electrical conductivity. These sensors are either metal oxide-based or conducting polymer sensors.[6–8] Conducting polymers have been found useful because of their advantages like easily tunable chemical structures, simple processing and promising morphologies compared to other materials. In this context, conjugated polymers and their nanocomposites have been proposed as active sensing materials to gain advantages in optoelectronic properties and better sensitivity towards a number of acidic or basic gases to be utilized in state-of-the-art devices and at room temperature operation. The high demand for analytical devices necessitates the development of smart technologies that enable faster and efficient detection of desired analytes. Currently, various device architecture combinations and improved methods of the existing technology platforms are being developed to enhance the analyte detection sensitivity and selectivity.[9–16] The main goal for the development of such devices is to achieve greater device performances in an affordable and less economic cost. Examples of analytical devices include portable and easily accessible glucose sensors used extensively in medical practices as well as for home testing. However, the development of such analytical devices involves a trade-off between the cost of production and device sensitivity. Hence, device improvements without compromising the sensitivity of the analytical device can be further explored. Organic electrochemical transistors (OECTs) are promising in this regard due to their low operating voltages, ability to work in aqueous environments and ease of fabrication. In addition, OECTs can detect desired analytes specifically through active

[a] Centre for Nanotechnology, Indian Institute of Technology, Guwahati 781039, Assam, India. E-mail: pki@iitg.ac.in
[b] Department of Chemistry, Indian Institute of Technology, Guwahati 781039, Assam, India

† Electronic supplementary information (ESI) available: FESEM & XRD data. See DOI: https://doi.org/10.1039/d2sd00099g

material functionalization or a chemical reaction involving the analytes as a reactant or by-product. Further, OECTs based on poly (3,4-ethylenedioxythiophene) doped with polystyrene sulfonate (PEDOT:PSS) can be integrated into microfluidic systems which are used for logic circuits. Such integration facilitates sensing of biomolecules such as glucose, deoxyribonucleic acid (DNA), neurotransmitters and certain other biomarkers. These devices follow the ion-to-electron converter mechanism, providing an effortless route to interface biology with electronics.[17–24]

Thus, these devices offer the advantage of detecting large changes in the electronic current even on a relatively small ionic drift. As such, herein, we have introduced a polyhydroxyl layer (PHD) to design a PEDOT:PSS based OECT for exploring its capability towards improved transistor performance. Apart from being selective to ammonia, the PHD layer also provides device stability, protects the transistor in an aqueous environment and provides room-temperature operation under ambient conditions. We have confirmed the presence of strong hydrogen bonds, N–H stretching and cavity condensation. Together, all these notable features along with the mesoporous nature of the PHD film contribute to achieving the remarkable response of the solution processed PHD-OECT towards ammonia at low operating voltages of <1 V. Table 1 represents a comparative study of room temperature ammonia detection using various techniques.

Experimental section

Materials and methods

PEDOT:PSS, acrylic acid, and 30% ammonia solution were purchased from Sigma-Aldrich. Glycerol was purchased from Merck and *p*-toluene sulfonic acid from LobaChemie. CV measurements were carried out using a CH instruments Model 700D series. Ag/AgCl was used as the reference electrode and 0.1 M NaCl as the aqueous electrolytic solution. The thickness of the deposited films was optimized using a Profilometer (Dektat-150). Field emission scanning electron microscopy (FESEM) images were recorded on a Sigma Carl ZEISS SEM instrument. FT-IR was recorded on a Perkin Elmer spectrometer with samples prepared using KBr pellets.

Synthesis

A polyhydroxyl derivative was synthesized by mixing 0.03 mol of glycerol, 0.09 mol of acrylic acid and 0.05 g of *p*-toluene sulfonic acid together for 30 min. A viscous solution was formed after mixing which was used for coating the device. The material has been found to be chemically, thermally, and mechanically stable for room temperature experiments which can be attributed to the cross-linked homogeneous texture.[25]

Sensor fabrication

Microscopic glass slides of dimensions 1 cm × 2 cm were utilized as substrates which were cleaned in piranha solution for 1 hour and washed several times with deionised water followed by sanitation prior to use. The cleaned substrates were then dried, ionized and subsequently 100 nm thickness aluminium contacts were thermally deposited on them inside the glove box. A channel of dimensions 30 mm length (L) and 2 mm width (W) was obtained which was used as the source (S) and drain (D). 30 nm thick PEDOT:PSS films were coated on these aluminium deposited substrates. The coated substrates were again heated at 130 °C for 1 hour. The synthesized polyhydroxyl layer was coated over the PEDOT:PSS region and heated at 50 °C for 30 minutes. An ammonia concentration of 1 μM was used for all the experiments.

Characterization

a. Electrical measurements

All the electrical characterizations of the devices were carried out under ambient conditions at room temperature using a Keithley2614B. A positive gate bias (V_g) was applied with the Ag/AgCl electrode and the two aluminium electrodes served as a source (S) and drain (D). The ammonia sensing experiments were performed at drain voltage $V_d = -0.2$ V with a gate voltage V_g sweep ranging from 0 to 1 V in 5 ml electrolyte solution at pH = 7. The analyte and ammonia solutions were confined in a 10 mL beaker and mixed with the electrolyte prior to testing.

b. Field emission scanning electron microscopy (FESEM) and X-ray diffraction (XRD)

FESEM images of the PHD film on glass slides were recorded on a Sigma Carl ZEISS scanning electron microscope at an accelerating voltage of 15 kV at different magnifications. XRD was recorded on a Bruker D8 Advance model (provided in ESI†).

c. Brunauer–Emmett–Teller (BET) and Barrett–Joyner–Halenda (BJH)

BET/BJH experiments of PHD were performed on an Autosorb-IQ MP instrument to understand the porosity of the selective layer.

d. Fourier transform infrared analysis (FT-IR)

FT-IR was recorded on a Perkin Elmer spectrometer with solid samples prepared using KBr pellets. Selected IR peaks with tentative assignments (n_{max}/cm^{-1}) were recorded.

Results and discussion

a. Electrical measurements

The OECT and polyhydroxyl derivative used for coating are shown in Fig. 1a. The electronic transfer characteristic is indicated at $V_d = -0.2$ V and drain characteristics at different gate voltages are shown in Fig. 1b. The measurements were done under positive gate bias which subsequently changes the channel conductance through injection of ions from the aqueous medium. This process, in turn, affects the

Table 1 A comparative study of room temperature ammonia detection considering varied techniques

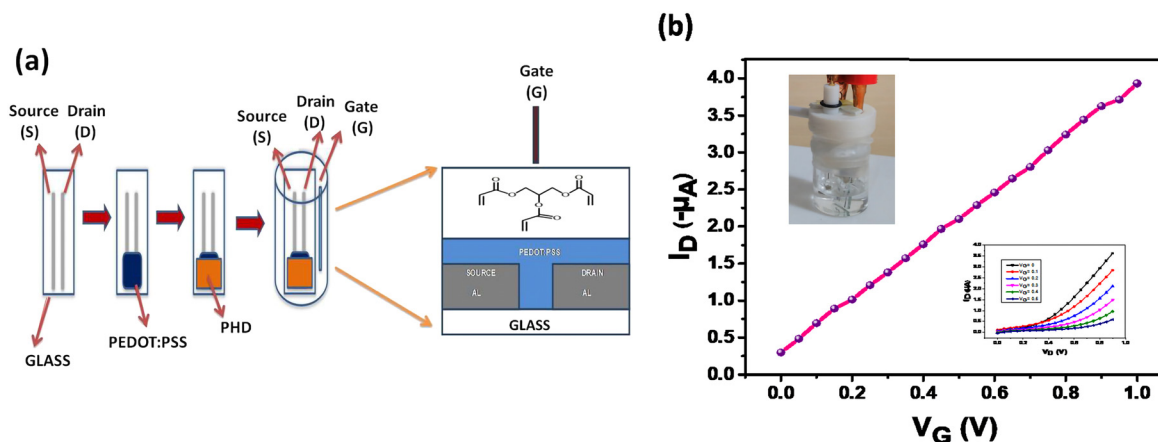| Sl no.	Ref.	Active material	Detection method	Temperature	LOD
1.	Hussain et al., [15a] Anal. Chem., 2016, 88, 12453–12460	Ionic liquid (RTIL) 1-ethyl-3-methylimidazolium bis(trifluoromethylsulfonyl)imide([C2mim]-[NTf2])/microarray thin film electrode (MATFE)	Voltammetric	Room temperature	0.1 to 2 ppm
2.	Macklin et al., [14a] ACS Appl. Mater. Interfaces, 2018, 10, 16169–16176	Graphene	Chemiresistive	Room temperature	160 ppm
3.	Kannan et al., [16] J. Mater. Chem. A, 2014, 2, 394	α-Fe_2O_3	Impedimetric	Room temperature	100–1000 ppm
4.	Meng et al., [11b] J. Mater. Chem. A, 2015, 3, 1174	Cu_2O nanorods/rGO	Surface-controlled Adsorption	Room temperature	200 ppm
5.	Ghosh et al., [36]	RGO–SnO_2 hybrid	Conducting hetero junctions	Room temperature	25–2800 ppm
6.	Kim et al., [11a] J. Mater. Chem. A, 2017, 5, 19116	Chemically fluorinated graphene oxide (CFGO)	Chemoresistive	Room temperature	100–500 ppb
7.	Wang et al., [37]	SnO_2/bionic porous (BP) carbon composites	Microwave transduction technology	Room temperature	10–200 ppm
8.	Singh et al., [38]	$MoSe_2$ crystalline nanosheets	Resistive	Room temperature	1 ppm
9.	Kanaparthi et al., [39]	Polyaniline (PANI)	Chemiresistive	Room temperature	200 ppb to 3.15 ppm
10.	Seelkaew et al., [40]	Sn–TiO_2@rGO/CNT	Resistive	Room temperature	250 ppm
11.	Murugappan et al., [13b] Electrochem. Commun., 2011, 13, 1435–1438	Room temperature ionic liquids (RTILs)	Electrochemical	Room temperature	50 ppm and 185 ppm
12.	Liu et al., [41]	Biomass hydrogel poly-L-glutamic acid and L-glutamic acid (PGA/GA)	Impedance	Room temperature	0.5 ppm
13.	Yin et al., [42]	Mesoporous NiO	Resistive	Room temperature	0.001 ppm (1 ppb)
14.	Chen et al., [43]	Core-shell Au@SiO_2 nanocrystals doped PANI	Resistive	Room temperature	10 ppb
15.	Tang et al., [44]	Graphene oxide (GO)	Love mode surface acoustic wave (SAW)	Room temperature	500 ppb
16.	Song et al., [45]	Ultrathin silicon nanowires (SiNWs)	Field-effect transistor	Room temperature	100 ppb
17.	Garg et al., [46]	Zeolite imidazole framework/reduced graphene oxide (ZIF-67/rGO) composite	Chemoresistive	Room temperature	74 ppb
18.	Present work	PEDOT:PSS/polyhydroxyl derivative (PHD)	Organic electrochemical transistor (OECT)	Room temperature	71.6 ppb

Fig. 1 Schematic illustration and digital image of the ammonia sensing device. a) Schematic drawing of the device showing various layers and incorporation of a mesoporous layer immersed in an electrolyte solution. b) Transfer characteristics (I_D–V_G) (inset top left device setup; inset down right output curves).

conductivity of the PEDOT:PSS layer which is referred to as doping/de-doping of PEDOT:PSS as depicted in eqn (1).

$$PEDOT^+:PSS^- + M^+ + e^- \rightleftharpoons PEDOT^0 + M^+:PSS^- \qquad (1)$$

where M^+ represents a cation and e^- an electron.

The transistor characteristics of the PHD-OECT are due to ions acting as charged carriers contributing to its high sensitivity. Therefore, these characteristics result in a built-in amplification entity (Fig. 1b). This system is found to be highly sensitive towards ammonia, *i.e.*, it forms an ammonia

sensitive layer. Hence, the presence of small concentration of ammonia is selectively detected. It is found that the electron transfer curve shifts significantly upon exposure to different concentrations of ammonia. Various analytes, such as urea, thiourea, ethanolamine, diethylamine, $FeCl_3$, hydrazine, NaCl and KCl, have been tested with this sensor assembly.

b. FESEM and XRD

The surface morphology of the PHD film layer before and after exposure to ammonia can be seen in Fig. S1(a–c) (ESI).† In Fig.
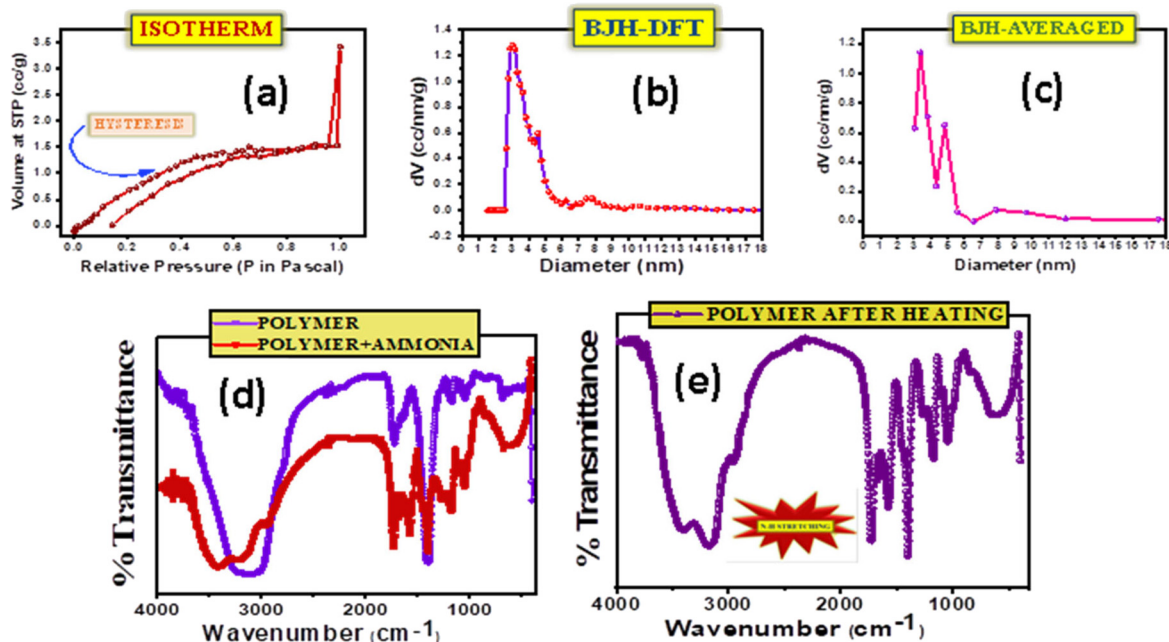

Fig. 2 Surface area evaluation for determination of pores as well as functional groups and characterizing chemical bond formation. a) Isotherm of a mesoporous PHD layer when exposed to nitrogen. b) Pore size distribution of PHD calculated using the BJH-DFT method. c) Pore size distribution of PHD calculated using the BJH-averaged method. d) FTIR analysis of PHD before and after exposure to ammonia. e) FTIR analysis of PHD after heating and exposure to ammonia resulting in N–H stretching.

S1a and S1b (ESI†), the PHD layer before exposure to ammonia at 100× and 500× magnification respectively shows well-defined grooves. Exposing it to ammonia changes the structural pattern (Fig. S1c).† The XRD data shows a shift of peaks after exposure to ammonia. Both in powder and film form, PHD is mostly amorphous in nature (Fig. S1d and S1e, ESI†). This could be one of the factors contributing to the PHD-OECT device's high performance at low operating voltages. However, the peak at 20.8° for PHD powder (Fig. S1d, ESI†) shows a shift to 28.48° after exposure to ammonia. Similarly, the peak at 23.04° for the PHD film (Fig. S1e, ESI†) shows a shift to 32.08° after exposure to ammonia (provided in the ESI†).

c. Brunauer–Emmett–Teller (BET) and Barrett–Joyner–Halenda (BJH)

The adsorption and desorption of N_2 in an isotherm determines the presence of pores in the material and the likeable cavity condensation. The appearance of hysteresis highlights the presence of mesoporous pores in the material (Fig. 2a). Since pores of a specific size are filled at higher pressures and expelled at lower pressures, cavity condensation takes place during adsorption; and cavity evaporation takes place during desorption. The BET experiment performed on the samples revealed the porosity of the selective layer. In Fig. 2b and c, the pore distributions of the selective layer are observed which is in direct contact with the electrolyte. Fig. 2b shows the pore size distribution calculated through the DFT method, while in Fig. 2c it is an averaged data. In both figures, the presence of different pore sizes is observed; however, a maximum of 3 nm pore size was noticed. Thus, the ions in the electrolyte could easily pass through the porous selective layer to dope or de-dope the PEDOT:PSS layer. Although it is possible for the ions of the analyte to infiltrate the layer, the selectivity factor, along with attraction and repulsion forces, comes into play and allows more ammonium ions to be detected.[26–28]

d. Fourier transform infrared (FT-IR) analysis

FT-IR analysis performed at room temperature on the selective layer (Fig. 2d and e) on pristine and after ammonia exposure confirmed the changes occurring after the addition of ammonia and revealed broad peaks at ~3406 cm^{-1} for PHD w. r.t. 3138 cm^{-1} for PHD without ammonia corresponding to the –OH groups. The peaks at 3172 cm^{-1} and 2947 cm^{-1} present in PHD with ammonia are not seen in PHD without ammonia, and the peaks at 1732 cm^{-1} for PHD without ammonia and at 1724 cm^{-1} for PHD with ammonia confirm the formation of ester. The idea of detecting a hydrogen bond (HB) solely on one single site can be done by quantum chemical calculation. However, the prediction of H-bonding can be made by observing the easily accessible basic sites of PHD for interacting with NH_3. First, we assume that the interaction with these sites results in H-bonded complexes. It could also be demonstrated from the classification of acceptor atom types in order to form hydrogen-bonded complexes and also for

forming more effective sites. In this context, three regions may be recommended to associate with NH_3 through hydrogen bonds with specific acceptor atoms, say –C–O–C– and –C=O. Accordingly the utility of these sites as a criterion for sensing of NH_3 through H-bonds can be understood. These groups can be connected to a H-atom of NH_3 by a HB and the strength of the bond as well as the sensitivity depends on the electron density of these groups to attract hydrogen. HBs are ubiquitous in this structure and have been the important focus in sensing processes. Many studies have shown that sensing mechanisms can be well-explained by HB interactions.[29–34] The probe PHD shown in Fig. 2d and e, taken by the IR vibration analysis before and after interaction with NH_3, shows that all the relevant vibrational peaks are distinctly shifted. The FTIR spectra of functional groups, –C=O, –C–O–C– and H–N related to HBs, show the red-shift in vibration frequencies of up to 268 cm^{-1} (3406 → 3138 cm^{-1}) (Fig. 2d and e). This red shift indicates the existence of a hydrogen bond (HB), whereas the blue shift indicates its weakening. Analysis of sensing mechanisms can be demonstrated from the six nucleophilic sites of PHD. Out of these sites, the most electronegative sites attract the H of NH_3 although these sites cannot be distinguished from experimental results. Thus, the vibrational spectra confirm the mechanism of HB in the ground state. The presence of hydrogen bonding between the –C=O group of PHD and ammonia results in an increase of –C=O as well as H–N bond length. Fundamentally, the vibrational frequency for these bonds will decrease leading to a change in IR stretching frequencies of –C=O (PHD) and H–N (ammonia). The IR spectra of PHD after addition of ammonia have also been examined. On heating for 20 minutes the IR spectra were again taken, showing a slight impression of ammonia in the spectra. In Fig. 2e, the difference after application of heat could be ascertained. The original IR of PHD could be observed with N–H stretching at 3175 cm^{-1} which was not found before exposure to ammonia. This can be attributed to the formation of strong hydrogen bonds between PHD and ammonia. It proves stable hydrogen bond formation between –C=O (PHD) and ammonia at the exposed –C=O groups of the material. Moreover, the formation of hydrogen bonds may weakly polarise the ammonia molecule which can facilitate the accumulation of more NH_3 molecules inside the pores of the material and thereby induce cavity condensation. Thus, both hydrogen bonding and cavity condensation operate in this system. The possibility of reversibility in this configuration indicates that the device can be reusable with a baseline correction. Aggregation of NH_3 at the nucleophilic sites *i.e.* –C=O and –C–O–C– can significantly affect the extent of reactivity or selectivity at these regions. Here, the presence of NH_3 in IR spectra on heating reveals the importance of H-bond networks where it forms a strong HB with the analyte.

Gaussian studies

The structure of the PHD derivative may be analysed in three subunits I, II and III (Fig. 3a). The configuration of subunits I
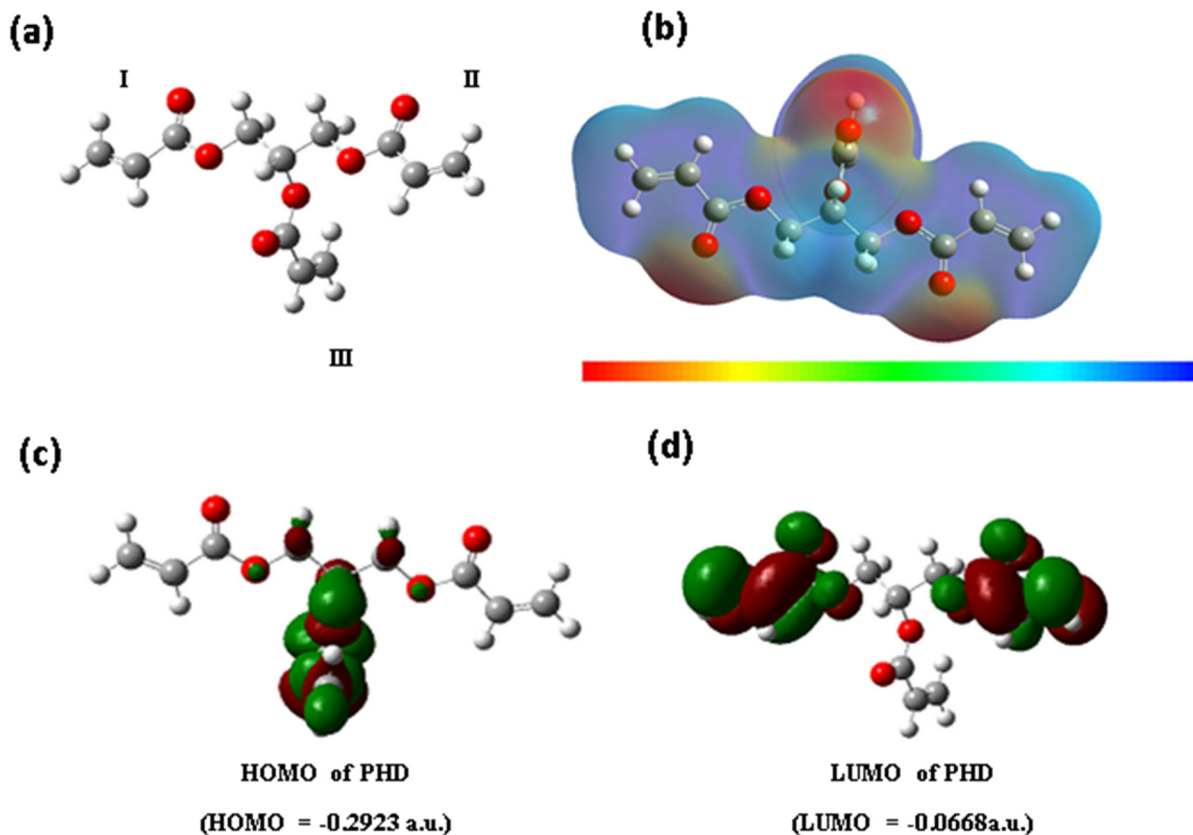
Fig. 3 Computational study and molecular electronic structure calculations of PHD. a) Gaussian model of the 3D structure of PHD with three acrylate subunits. b) Electronic cloud density distribution of PHD. c) HOMO of PHD. d) LUMO of PHD.

and II remains along the same axial plane, whereas unit III lies perpendicular to this plane. The acrylate groups are bonded to primary carbon centres in subunits I and II, whereas in subunit III the acrylate group is attached to the tertiary carbon centre through a carboxylate bond. Hence, the nature of electrostatic potential around this monomer PHD may indicate distinguishable variation in electron density. The completely optimized polyhydroxyl derivative with the B3LYP/6-31G(d,p) method was used for calculating electrostatic potential (Fig. 3b). Thus, we have computed the EPS profile in the 3D structure of monomer PHD.

More negative values are found around $-C\!\!=\!\!O$ of these three regions and less negative or positive values are found around the rest of the regions. The maximum negative value in regions I and II is approximately -4.31×10^{-2} a.u., whereas the value for region III is -4.58×10^{-2} a.u. Hence, region III may be more perceptive of NH_3 or NH_4OH (in aqueous solution) than regions I and II. This may be the reason why the PHD material is very sensitive towards NH_3 or NH_4OH (in aqueous solution).The electron labile property of the polyhydroxyl derivative can be related to the energy gap of frontier orbitals, *i.e.* HOMO–LUMO (Fig. 3c). The optimized structure of the PHD derivative using B3LYP/6-31G(d,p) was used for calculating the HOMO and LUMO energies and Fig. 3c and d show the electron density distribution. The HOMO–LUMO gap is found to be −6.1 eV, but the value is

much larger for an electronically conductive material. According to the electronic property of the PHD derivative, $-C\!\!=\!\!C-$ and $-C\!\!=\!\!O$ groups generally undergo n–π* and π–π* transitions, but such transitions occur only in the excited states. Hence, electronic conduction may not occur in the process of NH_3 or NH_4OH (in aqueous solution) sensing. It is essential to analyse electrostatic potential in the 3D structure of the polyhydroxyl derivative.

Sensing mechanism

The sensing of a transistor is based on integration of ions in aqueous solution repelled by the positively charged gate and attracted by the negative channel. The species sensed acquires a positive charge in aqueous medium which then associates with the polyhydroxyl layer and gets absorbed by it to further de-dope the PEDOT:PSS polymer film to create changes in the *I–V* characteristics of the device. The absorption/association with the acrylate polymer film involves different intermolecular interactions like H-bonding, dipolar interaction, London forces, dispersion forces and individual ionic conductivities of ions furnished by various species taken into consideration. In this study, we have analysed a large set of species commonly found in industrial wastes and biological processes, such as ammonia, urea, thiourea, diethylamine (DA), ethanolamine (EA), hydrazine, and ionic
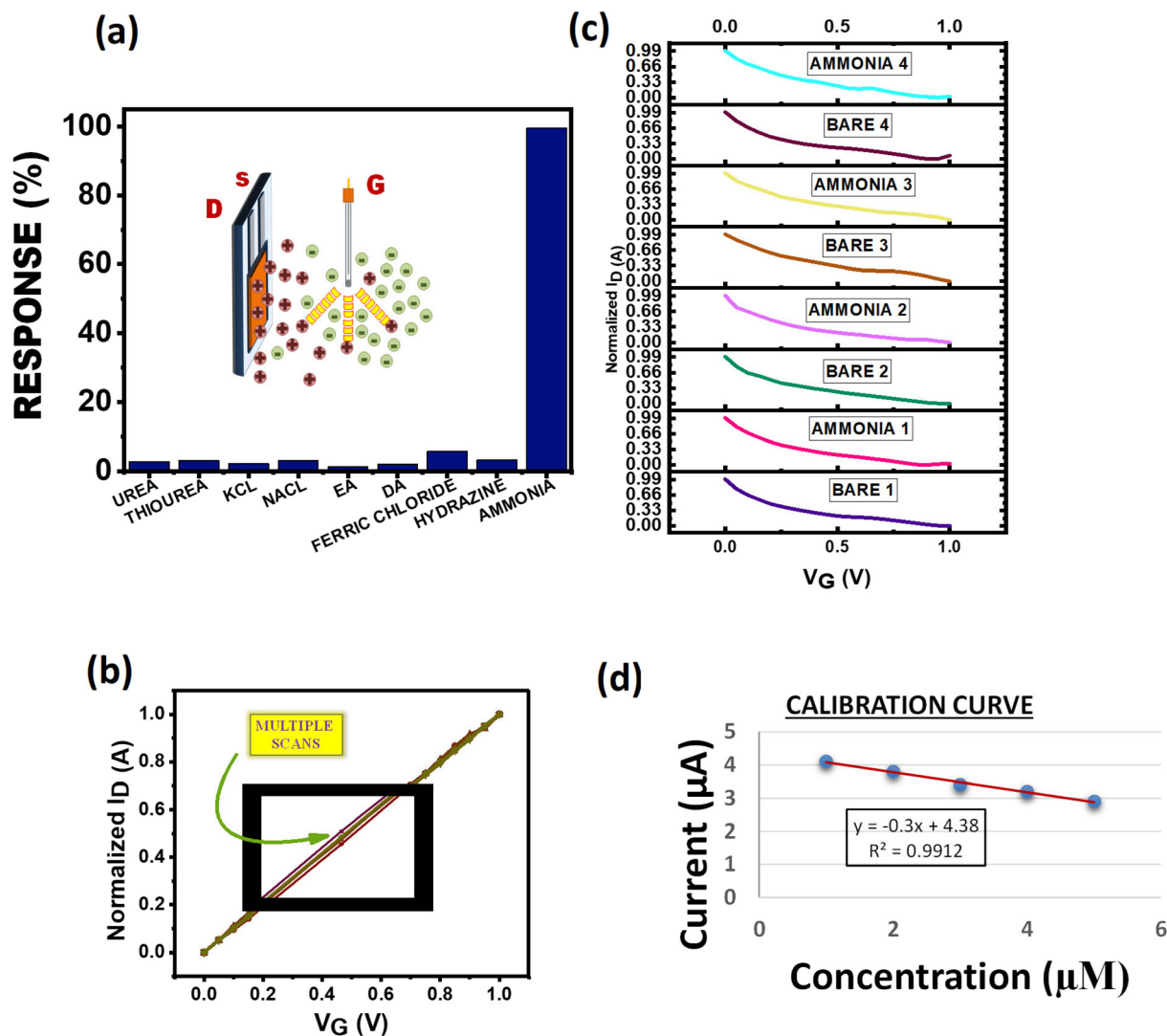
Fig. 4 Response of PHD-OECT to common industrial and biological waste products. a) Sensitivity of PHD compared to other analytes. b) Repeatability of the device kept in electrolytic solution. c) Analysing different devices in the same electrolytic solution. d) Calibration curve of the PHD modified device after exposure to ammonia.

salts like NaCl, KCl, and FeCl₃ in order to extract the highest sensitivity. The sensitivity profiles of these species depend on attraction forces, repulsion forces, and different intermolecular interactions between the acrylate polymer and ions furnished by the species taken into consideration. As per the results obtained in the process, ammonia shows the maximum sensitivity due to H-bonding between the acrylate and NH_3 which after absorption through the polymer film de-dopes the PEDOT:PSS polymer up to the maximum extent (Fig. 4a). In ionic cases like NaCl and KCl the sensitivity is lower due to poor interaction between the polymer and Na^+/K^+ ions. The sensitivity profile clearly shows approximately similar values for NaCl and KCl which can be explained on the basis of almost similar ionic properties and dissociation of both salts in water. As NaCl is slightly more soluble in water hence it shows a higher value than KCl. In the case of ionic salts like $FeCl_3$, due to higher solubility than NaCl and KCl, $FeCl_3$ shows a slightly higher sensitivity but the overall

sensitivity when compared to NH_3 is fairly low due to rapid complexation of Fe^{3+} ions with water molecules to form $[Fe(H_2O)_6]^{3+}$ hexaaquairon(III) complex ions. Hence, the interaction of Fe^{3+} has been reduced with the sensing polymer layer which led to the sensitivity profile seen in Fig. 4a. In the case of other organic samples taken into consideration for this study, namely urea and thiourea molecules, due to the high electronegativity of oxygen (O) in the urea molecule polarisation takes place leading to lower electron density on both $-NH_2$ groups. This results in less association of the urea molecule with the acrylate group as indicated by the reduced sensitivity of urea as compared to thiourea. However, overall they have a very high tendency to form hydrogen bonding with the polymer; hence their sensing profile is high as compared to those of other organic samples. In the case of hydrazine, the molecule exists as $NH_2-NH_3^+$ in water which will associate with the polymer but repulsions due to a nearby second $-NH_2$ group led to lower sensitivity than ammonia,

urea and thiourea but can be comparable to that of ionic salts like KCl and NaCl. The sensitivity of ethanolamine is least as compared to the rest due to the presence of intra-molecular hydrogen bonding between the –OH group and –NH_2 group which will result in less association of ethanolamine with the acrylate group of the PHD layer. In the case of diethylamine, the association is somewhat more due to the absence of such an electron rich group. It is less repelled and more associated to the polymer as compared to ethanolamine as seen in the sensitivity profile.

Repeatability and reproducibility are two distinguised features in a sensor. The device characteristics were measured for the same device multiple times in the same electrolyte solution (Fig. 4b). The device does not deter away from its original value and is repeatable even after successive 10 scans. Four different devices fabricated under the same conditions scanned in the same electrolyte solution indicate that our device is reproducible (Fig. 4c). The values for different concentrations of ammonia were plotted to get the calibration curve for the calculation of the limit of detection (LOD) (Fig. 4d). Increasing concentration of ammonia is injected into the electrolyte solution where the device is immersed as seen in Fig. 1a and the LOD was calculated to be 71.6 ppb. Exposure to ammonia of about 25 ppm for 8 hours is hazardous to health.[35] As such, this approach to fabricate OECTs could be further explored for improved detection of various analytes in a cost-effective manner.

Conclusion

In conclusion, a mesoporous film platform using a vertical OECT has been developed utilizing poly(3,4-ethylenedioxythiophene) doped with polystyrene-sulfonate (PEDOT:PSS), and ammonia sensing at the 71.6 ppb level has been achieved. We have demonstrated that the sensor assembly has excellent transistor characteristics and can be operated with voltages <1 V. The polyhydroxyl film is optimal in an aqueous environment at room temperature due to its cross-linked homogeneous texture. The developed PHD-OECT is highly sensitive and selective for ammonia with the presence of strong hydrogen bond formation and N–H stretching. It has been observed that there were mesoporous pores on the PHD film that enhance the sensing attributes of PHD-OECT towards ammonia with excellent electrical response. Due to the economic viability of this PHD-OECT sensor, the present approach can be further explored to detect other biological and chemical analytes efficiently.

Conflicts of interest

The authors declare that the research was conducted in the absence of conflict of interest.

Acknowledgements

References

1 (a) B. Timmer, W. Olthuis and A. van den Berg, *Sens. Actuators, B*, 2005, **107**, 666–677; (b) J. F. M. Oudenhovena, W. Knobena and R. van Schaijka, *Procedia Eng.*, 2015, **120**, 983–986; (c) R. A. Michaels, *Environ. Health Perspect.*, 1999, **107**, 617–627; (d) D. Leduc, P. Gris, P. Lheureux, P. A. Gevenois, P. De Vuyst and J. C. Yernault, *Thorax*, 1992, **47**, 755–757.

2 (a) J.-C. Jin, J. Wu, G.-P. Yang, Y.-L. Wu and Y.-Y. Wang, *Chem. Commun.*, 2016, **52**, 8475–8478; (b) A. Kalita, S. Hussain, A. H. Malik, U. Barman, N. Goswami and P. K. Iyer, *ACS Appl. Mater. Interfaces*, 2016, **8**, 25326–25336; (c) N. Sharma, N. Sharma, P. Srinivasan, S. Kumar, J. B. B. Rayappan and K. Kailasam, *J. Mater. Chem. A*, 2018, **6**, 18389; (d) L. R. Adil, P. Gopikrishna and P. K. Iyer, *ACS Appl. Mater. Interfaces*, 2018, **10**, 27260–27268.

3 (a) T. Someya, Z. Bao and G. G. Malliaras, *Nature*, 2016, **540**, 379–385; (b) M. Berggren and A. Richter-Dahlfors, *Adv. Mater.*, 2007, **19**, 3201–3213; (c) N. Zehra, D. Dutta, A. H. Malik, S. S. Ghosh and P. K. Iyer, *ACS Appl. Mater. Interfaces*, 2018, **10**, 27603–27611.

4 (a) T. Grady, T. Butler, B. D. MacCraith, D. Diamond and M. A. McKervey, *Analyst*, 1997, **122**, 803–806; (b) W. Cao and Y. Duan, *Sens. Actuators, B*, 2005, **110**, 252–259.

5 Z. Jin, Y. Su and Y. Duan, *Sens. Actuators, B*, 2001, **72**, 75–79.

6 (a) N. R. Stradiotto, H. Yamanaka and M. V. B. Zanoni, *J. Braz. Chem. Soc.*, 2003, **14**(2), 159–173; (b) U. Yogeswaran and S.-M. Chen, *Sensors*, 2008, **8**, 290–313; (c) G. Saikia, A. K. Dwivedi and P. K. Iyer, *Anal. Methods*, 2012, **4**, 3180–3186.

7 (a) F. Rigoni, S. Tognolini, P. Borghetti, G. Drera, S. Pagliara, A. Goldoni and L. Sangaletti, *Analyst*, 2013, **138**, 7392–7399; (b) A. Kalita, S. Hussain, A. H. Malik, N. V. V. Subbarao and P. K. Iyer, *J. Mater. Chem. C*, 2015, **3**, 10767–10774.

8 (a) P. K. Sekhar and J. S. Kysar, *J. Electrochem. Soc.*, 2017, **164**(4), 113–117; (b) N. Zehra, A. Kalita, A. H. Malik, U. Barman, M. A. Afroz and P. K. Iyer, *ACS Sens.*, 2019, **5**, 191–198.

9 (a) S. Stříteský, A. Marková, J. Víteček, E. Šafaříková, M. Hrabal, L. Kubáč, L. Kubala, M. Weiter and M. Vala, *J. Biomed. Mater. Res., Part A*, 2018, **106**(4), 1121–1128; (b) V. Rani and K. S. V. Santhanam, *J. Solid State Electrochem.*, 1998, **2**, 99–101.

10 (a) M. Chen, D. Nilsson, Th. Kugler and M. B. T. Remonen, *Appl. Phys. Lett.*, 2002, **81**(11), 2011–2013; (b) C.-S. Lee, S. K. Kim and M. Kim, *Sensors*, 2009, **9**, 7111–7131; (c) S. Mondal, N. Zehra, A. Choudhury and P. K. Iyer, *ACS Appl. Bio Mater.*, 2020, **4**, 47–70; (d) N. Meher, S. R. Chowdhury and P. K. Iyer, *J. Mater. Chem. B*, 2016, **4**, 6023–6031; (e) N. Meher and P. K. Iyer, *Nanoscale*, 2017, **9**, 7674–7685.

11 (a) Y. H. Kim, J. S. Park, Y.-R. Choi, S. Y. Park, S. Y. Lee, W. Sohn, Y.-S. Shim, J.-H. Lee, C. R. Park, Y. S. Choi, B. H. Hong, J. H. Lee, W. H. Lee, D. Lee and H. W. Jang, *J. Mater. Chem. A*, 2017, **5**, 19116–19125; (b) H. Meng, W. Yang, K. Ding, L. Feng and Y. Guan, *J. Mater. Chem. A*, 2015, **3**, 1174–1181.

12 (a) S. Pandey, G. K. Goswami and K. K. Nanda, *Sci. Rep.*, 2013, **3**, 2082; (b) S. Arya, M. Riyas, A. Sharma, B. Singh, Prerna, P. Bandhoria, S. Khan and V. Bharti, *Appl. Phys. A: Mater. Sci. Process.*, 2018, **124**, 538; (c) A. S. Tanwar, S. Patidar, S. Ahirwar, S. Dehingia and P. K. Iyer, *Analyst*, 2019, **144**, 669–676; (d) S. Hussain, A. H. Malik and P. K. Iyer, *ACS Appl. Mater. Interfaces*, 2015, **7**, 3189–3198.

13 (a) S. C. Hernandez, D. Chaudhuri, W. Chen, N. V. Myung and A. Mulchandani, *Electroanalysis*, 2007, **19**, 2125–2130; (b) K. Murugappan, J. Lee and D. S. Silvester, *Electrochem. Commun.*, 2011, **13**, 1435–1438.

14 (a) C. Mackin, V. Schroeder, A. Zurutuza, C. Su, J. Kong, T. M. Swager and T. Palacios, *ACS Appl. Mater. Interfaces*, 2018, **10**, 16169–16176; (b) N. Meher and P. K. Iyer, *Angew. Chem., Int. Ed.*, 2018, **57**, 8488–8492.

15 (a) G. Hussain and D. S. Silvester, *Anal. Chem.*, 2016, **88**, 12453–12460; (b) A. Dey, A. Singh, D. Das and P. K. Iyer, *Phys. Chem. Chem. Phys.*, 2016, **18**, 32602–32609.

16 P. K. Kannan and R. Saraswathi, *J. Mater. Chem. A*, 2014, **2**, 394.

17 H. S. White, G. P. Kittlesen and M. S. Wrighton, *J. Am. Chem. Soc.*, 1984, **106**, 5375–5377.

18 D. A. Bernards, G. G. Malliaras, G. E. S. Toombes and S. M. Gruner, *Appl. Phys. Lett.*, 2006, **89**, 053505–053508.

19 (a) A. Dey, A. Singh, D. Dutta, S. S. Ghosh and P. K. Iyer, *J. Mater. Chem. A*, 2019, **7**, 18330–18337; (b) S. Pecqueur, S. Lenfant, D. Guérin, F. Alibart and D. Vuillaume, *Sensors*, 2017, **17**, 57.

20 (a) M. Ghittorelli, L. Lingstedt, P. Romele, N. I. Crăciun, Z. M. Kovács-Vajna, P. W. M. Blom and F. Torricelli, *Nat. Commun.*, 2018, **9**, 1441–1451; (b) M. J. Donahue, A. Williamson, X. Strakosas, J. T. Friedlein, R. R. McLeod, H. Gleskova and G. G. Malliaras, *Adv. Mater.*, 2018, **30**, 1705031–1705035.

21 N. Stutzmann, R. H. Friend and H. Sirringhaus, *Science*, 2003, **299**, 1881–1884.

22 M. Uno, Y. Tominari and J. Takeya, *Appl. Phys. Lett.*, 2008, **93**, 173301–173303.

23 J. Rivnay, P. Leleux, M. Ferro, M. Sessolo, A. Williamson, D. A. Koutsouras, D. Khodagholy, M. Ramuz, X. Strakosas, R. M. Owens, C. Benar, J.-M. Badier, C. Bernard and G. G. Malliaras, *Sci. Adv.*, 2015, **1**, 1400251–1400255.

24 M. Demelas, E. Scavetta, L. Basiricò, R. Rogani and A. Bonfiglio, *Appl. Phys. Lett.*, 2013, **102**, 193301–193304.

25 P. Dutta, B. Kalita, B. Gogoi and N. Sen Sarma, *J. Phys. Chem. C*, 2015, **119**, 17260–17270.

26 R. Bardestani, G. S. Patience and S. Kaliaguine, *J. Chem. Eng.*, 2019, **97**, 2781–2791.

27 P. Kuhn, A. Forget, D. Su, A. Thomas and M. Antonietti, *J. Am. Chem. Soc.*, 2008, **130**, 13333–13337.

28 J. C. Groen, L. A. A. Peffer and J. Pérez-Ramírez, *Microporous Mesoporous Mater.*, 2003, **60**, 1–17.

29 R. J. C. Brown, *J. Mol. Struct.*, 1995, **345**, 77–81.

30 B. Kojić-Prodić and K. Molčanov, *Acta Chim. Slov.*, 2008, **55**, 692–708.

31 A. D. Buckingham, J. E. Del Bene and S. A. C. McDowell, *Chem. Phys. Lett.*, 2008, **463**, 1–10.

32 P. A. Colman and L. C. Allen, *Chem. Rev.*, 1972, **72**, 283–303.

33 M. C. Etters, *Acc. Chem. Res.*, 1990, **23**, 120–126.

34 I. V. Alabugin, M. Manoharan, S. Peabody and F. Weinhold, *J. Am. Chem. Soc.*, 2003, **125**, 5973–5987.

35 T. N. I. F. O. S. A. H. (NIOSH), *Ammonia*, **https://www.cdc.gov/niosh/pel88/7664-41.html.**

36 R. Ghosh, A. K. Nayak, S. Santra, D. Pradhan and P. Kumar Guha, *RSC Adv.*, 2015, **5**, 50165.

37 N. Wang, N. Zhang, T. Wang, F. Liu, X. Wang, X. Yan, C. Wang, X. Liu, P. Sun and G. Lu, *Sens. Actuators, B*, 2022, **350**, 130854.

38 S. Singh, J. Deb, U. Sarkar and S. Sharma, *ACS Appl. Nano Mater.*, 2020, **3**, 9375–9384.

39 S. Kanaparthi and S. G. Singh, *Org. Electron.*, 2019, **68**, 108–112.

40 Y. Seekaew, W. Pon-On and C. Wongchoosuk, *ACS Omega*, 2019, **4**, 16916–16924.

41 L. Liu, T. Fei, X. Guan, X. Lin, H. Zhao and T. Zhang, *Sens. Actuators, B*, 2020, **320**, 128318.

42 M. Yin and Z. Zhu, *J. Alloys Compd.*, 2019, **789**, 941–947.

43 G. Chen, Y. Yuan, M. Lang, Z. Lv, W. Ma, N. Gu, H. Liu, J. Fang, H. Zhang and Y. Cheng, *Appl. Surf. Sci.*, 2022, **598**, 153821.

44 Q. B. Tang, Y. J. Guo, Y. L. Tang, G. D. Long, J. L. Wang, D. J. Li, X. T. Zu, J. Y. Ma, L. Wang, H. Torun and Y. Q. Fu, *J. Mater. Sci.*, 2019, **54**, 11925–11935.

45 X. Song, R. Hu, S. Xu, Z. Liu, J. Wang, Y. Shi, J. Xu, K. Chen and L. Yu, *ACS Appl. Mater. Interfaces*, 2021, **13**, 14377–14384.

46 N. Garg, M. Kumar, N. Kumari, A. Deep and A. L. Sharma, *ACS Omega*, 2020, **5**, 27492–27501.